CDC42EP4, a perisynaptic scaffold protein in Bergmann glia, is required for glutamatergic tripartite synapse configuration

Natsumi Ageta-Ishihara[1], Kohtarou Konno[2], Maya Yamazaki[3], Manabu Abe[3], Kenji Sakimura[3], Masahiko Watanabe[2], Makoto Kinoshita*[,1]

[1] Department of Molecular Biology, Division of Biological Sciences, Nagoya University Graduate School of Science, Nagoya 464-8602, Japan

[2] Department of Anatomy, Hokkaido University Graduate School of Medicine, Sapporo 060-8638, Japan

[3] Department of Cellular Neurobiology, Brain Research Institute, Niigata University, Niigata 951-8585, Japan

*Correspondence to: Makoto Kinoshita at Department of Molecular Biology, Nagoya University Graduate School of Science, Furo, Chikusa, Nagoya 464-8602, Japan
Tel/Fax: +81.52.789.3653
Email: kinoshita.makoto@c.mbox.nagoya-u.ac.jp

Email addresses of the other authors:
NAI: ageta-ishihara.natsumi@h.mbox.nagoya-u.ac.jp
KK: kotoro@med.hokudai.ac.jp
MY: Maya.Yamazaki@ucsf.edu
MA: manabu@bri.niigata-u.ac.jp
KS: npsaki01@bri.niigata-u.ac.jp
MW: watamasa@med.hokudai.ac.jp

Abstract

Configuration of tripartite synapses, comprising the pre-, post-, and peri-synaptic components (axon terminal or bouton, dendritic spine, and astroglial terminal process), is a critical determinant of neurotransmitter kinetics and hence synaptic transmission. However, little is known about molecular basis for the regulation of tripartite synapse morphology. Previous studies showed that CDC42EP4, an effector protein of a cell morphogenesis regulator CDC42, is expressed exclusively in Bergmann glia in the cerebellar cortex, that it forms tight complex with the septin heterooligomer, and that it interacts indirectly with the glutamate transporter GLAST and MYH10/nonmuscle myosin IIB. Scrutiny of *Cdc42ep4*$^{-/-}$ mice had revealed that the CDC42EP4-septins-GLAST interaction facilitates glutamate clearance, while the role for CDC42EP4-septins-MYH10 interaction has remained unsolved. Here, we find anomalous configuration of the tripartite synapses comprising the parallel fiber boutons, dendritic spines of Purkinje cells, and Bergmann glial processes in *Cdc42ep4*$^{-/-}$ mice. The complex anomalies include 1) recession of Bergmann glial membranes from the nearest active zones, and 2) extension of nonactive synaptic contact around active zone. In line with the recession of Bergmann glial membranes by the loss of CDC42EP4, overexpression of CDC42EP4 in heterologous cells promotes cell spreading and partitioning of MYH10 to insoluble (*i.e.*, active) fraction. Paradoxically, however, *Cdc42ep4*$^{-/-}$ cerebellum contained significantly more MYH10 and N-cadherin, which is attributed to secondary neuronal response mainly in Purkinje cells. Given cooperative actions of N-cadherin and MYH10 for adhesion between neurons, we speculate that their augmentation may ~~account for~~ reflect the extension of nonactive synaptic contacts in *Cdc42ep4*$^{-/-}$ cerebellum. Transcellular mechanism that links the absence of CDC42EP4 in Bergmann glia to the augmentation of N-cadherin and MYH10 in neurons is currently unknown, but the phenotypic similarity to GLAST-null mice indicates involvement of the glutamate intolerance. Together, the unique phenotype of *Cdc42ep4*$^{-/-}$ mice provides a clue to novel molecular network underlying tripartite synapse configuration.

Keywords

tripartite synapse, Bergmann glia, Purkinje cells, MYH10/nonmuscle myosin ⅡB, septin, synaptic contact

Abbreviations

IB: immunoblot, IP: immunoprecipitation, KO: knockout, Sup: supernatant, WT: wild type.

'Highlights' (each < 85 characters, including spaces).

1) *Cdc42ep4*$^{-/-}$ mouse cerebellum contains anomalous glutamatergic tripartite synapses.

2) The anomalies include recession of Bergmann glial processes from the active zone.

3) The anomalies include aberrant extension of synaptic contact around active zones.

4) ~~Possible attenuation of MYH10 in Bergmann glia may underlie the process recession~~ The anomalies accompany an~~.~~ aberrant insolubilization of MYH10, but not MYH9.

5) Augmentations of MYH10 and N-cadherin may partly account for the neuronal anomalies.

Introduction

In glutamatergic tripartite synapses, three components of the presynaptic (axon terminal or bouton), postsynaptic (dendritic spine), and perisynaptic (astroglial process) domains are tightly coupled both physically and functionally (Araque et al., 1999; Halassa et al., 2007; Chen et al., 2008; Perea et al., 2009). However, neither developmental nor activity-dependent mechanism by which neuronal and glial components coordinately regulate mutual adhesion and local shape is well understood, due in part to variety of synapses, and a plethora of membrane-bound molecules and submembranous cytoskeletal molecules involved (Iino et al., 2001; Watanabe, 2002; Tai et al., 2008; Garrett and Weiner, 2009; Friedman et al, 2015).

In our previous study, we found that a Bergmann glia-selective CDC42 effector protein CDC42EP4 is in tight complex with filamentous heterooligomers of septins (SEPT2/4/5/7/11) beneath plasma membranes of Bergmann glial lamellar processes (Ageta-Ishihara et al., 2015). The glial component enwraps pre- and postsynaptic components of glutamatergic synapses, most of which are formed between the parallel fibers and Purkinje cells (Altman and Bayer, 1997). The CDC42EP4-septins complex physically associates with a few membrane-bound and submembranous proteins, two of which had been reported to interact with septins; a glial glutamate transporter GLAST (Kinoshita et al., 2004; Hagiwara et al., 2011) and nonmuscle myosin IIs (Joo et al., 2007). We also demonstrated that genetic loss of CDC42EP4 causes a series of events that include 1) biochemical dissociation of GLAST from septins, 2) delocalization of GLAST away from the synaptic active zone, presumably due to release from the septin-based scaffold, 3) loss of efficiency in glutamate-buffering/clearance, and 4) motor coordination/learning defects in mice, where 3) and 4) are significantly masked by adaptive compensatory mechanisms (Ageta-Ishihara et al., 2015). On the other hand, physiological role for the CDC42EP4-septins-MYH10/nonmuscle myosin IIB interaction in the perisynaptic domain, as with the mechanism underlying 2), remain unaddressed.

Five members of the mammalian CDC42EP family are highly variable in size, domain structure, and expression patterns (Joberty et al., 1999), predictive of diverse molecular functions and physiological roles. In fact, CDC42EP-mediated complex phenomena are represented by the following findings, some of which are apparently incompatible: 1) Overexpression of CDC42EP5/Borg3 (calculated mass, 15 kDa) interferes with spreading of a mouse fibroblast cell line NIH3T3 on substrate, while sparing cell shape of a dog epithelial cell line MDCK (Joberty et al., 1999, 2001). 2) Depletion of CDC42EP3/Borg5 (28 kDa) suppresses actomyosin contractility in fibroblasts *in vitro* (Calvo et al., 2015). 3) Genetic loss of CDC42EP3 affects

septin and actomyosin, perturbing endothelial cell migration and angiogenesis *in vivo* (Liu et al., 2014b). 4) Overexpression of CDC42EP4 (38 kDa) augments the motility of a human breast epithelial cell line MCF-10A depending on the phosphorylation-mediated dissociation from CDC42 (Zhao and Rotenberg, 2014).

On the basis of the above background, in this study we reassess the cerebellar molecular layer of *Cdc42ep4*$^{-/-}$ mice, focusing on the tripartite synapses comprising the parallel fiber boutons, Purkinje cell dendrites, and Bergmann glial lamellar processes. Electron microscopic analysis reveals anomalous configuration not only in the glial component, but also in the neuronal components despite glia-selective expression of CDC42EP4. Biochemical and cell biological analyses indicate a role for the CDC42EP4-septins-MYH10 axis in the perisynaptic glial configuration. We further explore molecular mechanism underlying the pre- and postsynaptic anomalies originated from the perisynaptic defects.

Results

Anomalous configuration of tripartite synapses in the cerebellar cortex of *Cdc42ep4*$^{-/-}$ mice

To explore morphological phenotype of *Cdc42ep4*$^{-/-}$ mice focusing on the cerebellar cortex, we visualized Bergmann glia with immunofluorescence for phosphoglycerate dehydrogenase (3PDGH, Fig. 1A-D) and Golgi silver impregnation stain (Supplemental Fig. S1). Since the morphology of Bergmann glia is highly variable by location and by sectioning angle, we withheld quantitative comparison on the arborization pattern between WT and *Cdc42ep4*$^{-/-}$ mice.

As a means of quantitative comparison at a higher resolution, we randomly selected corresponding regions in *Cdc42ep4*$^{-/-}$ and WT cerebellar cortices, and exhaustively observed asymmetric synapses with transmission electron microscopy (TEM). It has been established that they are mostly glutamatergic synapses comprising pre-, post-, and perisynaptic components, which correspond respectively to boutons or axon terminals of the parallel fibers from the cerebellar granule cells, dendritic spines of Purkinje cells, and lamellar processes of Bergmann glia (Altman and Bayer, 1997; Yamada et al., 2000). In *Cdc42ep4*$^{-/-}$ mice, postsynaptic density (PSD) of cerebellar cortical synapses were normal in length, as reported (Ageta-Ishihara et al., 2015). However, they exhibited aberrant configuration which appeared to be a combination of inseparable anomalies; 1) recession of Bergmann glial membrane from the nearest active zone, and 2) extension of the nonactive synaptic contact around an active zone (Fig. 1E, F). As the latter is unambiguously definable, we measured the distance from an edge of a PSD to the nearest point of Bergmann glial membrane facing the synaptic gap. The morphometry revealed that "nonactive" synaptic contact around the active zone was significantly extended in *Cdc42ep4*$^{-/-}$ mice as compared with those of WT littermates (Fig. 1G, H). The morphological anomalies in the tripartite synapses may account in part for the endophenotype of *Cdc42ep4*$^{-/-}$ mice; *i.e.*, delocalization of GLAST away from the active zone and the insufficient glutamate-buffering/clearance capacity (Ageta-Ishihara et al., 2015).

Expression of CDC42EP4 facilitates cell spreading

Previous *in vitro* and *in vivo* studies on CDC42EP family proteins indicated their common roles for cell morphogenesis and/or migration in association with the septin and actomyosin cytoskeletal systems (see **Introduction**). However, whether the retraction of Bergmann glial membrane is attributed to the loss of function of *Cdc42ep4* is not technically reproducible or testable *in vitro*, because isolated Bergmann glial cells do not develop characteristic lamellar processes in culture (Belvindrah et al., 2006), and common tissue culture cell lines do not express

CDC42EP4. Alternatively, we examined whether expression of CDC42EP4 could induce morphological changes in heterologous COS-7 (a monkey kidney-derived cell line) cells in culture. While GFP distributed diffusely both in the nucleus and cytoplasm, GFP-CDC42EP4 fusion protein localized to the cytoplasm. GFP-CDC42EP4-expressing cells covered significantly wider area than GFP-expressing control cells at 1 h after replating (~1.5x on average, Fig. 2A). The difference in the cell area diminished to statistically insignificant level by 3 h after replating (data not shown). Albeit artificial, these findings indicate that CDC42EP4 has positive effect on the spreading of heterologous cells in culture, as is largely compatible with previous reports on its paralogs, CDC42EP1 and CDC42EP3 (Liu et al., 2014b; Calvo et al., 2015).

Expression of CDC42EP4 promotes partitioning of MYH10 to the insoluble fraction

To explore the mechanism underlying the facilitation of cell spreading by exogenous CDC42EP4 expression, we conducted biochemical fractionation of the cell lysate followed by immunoblotting. We first examined MYH10 on the basis that 1) MYH10 is a ubiquitous, principal motor protein that generates contractile/tensile force in the cell cortex, hence a major determinant of cell shape (Sellers, 2000; Lo et al., 2004; Cai et al., 2006; Vicente-Manzanares et al., 2009), 2) MYH10 is dominant among two other nonmuscle myosin IIs (*i.e.*, MYH9/nonmuscle myosin IIA, MYH14/nonmuscle myosin IIC) in neural tissues (Betapudi, 2014), 3) MYH10, in conjunction with actin, is involved in the activity-dependent morphological remodeling of dendritic spines (*i.e.*, structural plasticity) (Rex et al., 2010), and 4) MYH10 is co-immunoprecipitated with the CDC42EP4/septin complex from mouse cerebellar lysate (Ageta-Ishihara et al., 2015).

COS-7 cells expressing GFP-CDC42EP4 contained significantly more (x ~2.6) MYH10 in the insoluble fraction than GFP-expressing control cells (Fig. 2B). Previous reports showed that MYH10 in the insoluble fraction of COS-7 cells corresponds to the active, contractile fraction incorporated in the actin-based cytoskeletal network (Moncman et al., 1993), and that SEPT2-MYH9 interaction facilitate actomyosin contraction as a scaffold for the phosphorylation of myosin light chain by ROCK/Rho-kinase (Joo et al., 2007). Thus, our *in vitro* findings with COS-7 cells collectively indicate that CDC42EP4 expression augments septin/MYH10/actin interaction, and cell spreading.

Accumulation and insolubilization of MYH10 in *Cdc42ep4*$^{-/-}$ cerebellum

Our *in vitro* results also agree with previous reports on the requirement of nonmuscle myosin IIs for the spreading of fibroblasts (Liu et al., 2014a). As the two major nonmuscle myosin IIs (MYH9 and MYH10) play distinct roles (Betapudi et al., 2006), we compared their amounts in

the soluble/insoluble (supernatant/pellet) fractions of cerebellar lysates from *Cdc42ep4*$^{-/-}$ and WT mice. The insoluble fraction of *Cdc42ep4*$^{-/-}$ cerebellar lysate contained significantly more MYH10, but not MYH9, than that of WT mice, while the amounts of MYH9 and MYH10 in the soluble fractions were comparable (Fig. 3A, B). These data, along with a trend of slight increment of β-actin in the insoluble fraction (Fig. 3C), indicate selective augmentation of MYH10 in *Cdc42ep4*$^{-/-}$ cerebellum. Intriguingly, no such difference by genotype was observed in 4-week-old pups (Fig. 3D), reflecting postdevelopmental nature of the phenotype. However, the negative correlation between CDC42EP4 and insoluble MYH10 found *in vivo* seems incompatible with the positive correlation suggested by the *in vitro* experiments with COS-7 cells.

The major source of MYH10 in the cerebellum is Purkinje cells

To reconcile the apparent discrepancy between the *in vitro* and *in vivo* findings, we attempted to identify the origins of MYH10 contained in the cerebellar lysate by visualizing the distribution of MYH10 in the cerebellum. The intensity of immunofluorescence signal for MYH10 was highest in the somata and dendrites of Purkinje cells, but much lower in Bergmann glial cell bodies and processes (Fig. 3E). These are in agreement with previous immunofluorescence and *in situ* hybridization data (Miyazaki et al., 2000; Ma et al., 2006; Allen Brain Atlas). There was no recognizable anomaly in the distribution patterns of MYH10 and SEPT4 in *Cdc42ep4*$^{-/-}$ cerebellum at least at this resolution (Fig. 3E).

To corroborate the results, we further conducted immunoprecipitation-immunoblot (IP-IB) analysis of cerebellar lysates from WT mice. Consistently, a neuron-selective septin subunit SEPT3 pulled down MYH10 more efficiently than SEPT4 (Bergmann glia-selective subunit) and CDC42EP4 (Fig. 4A-C). These data demonstrate that Purkinje cells, but not Bergmann glia, are the major source of MYH10 in the cerebellar cortex and the lysate. Since Purkinje cells do not express the *Cdc42ep4* gene at lease in mice (Ageta-Ishihara et al., 2015; Allen Brain Atlas and Geo database from NCBI), we reasoned that dysfunctional *Cdc42ep4*$^{-/-}$ Bergmann glia transcellularly impinge on Purkinje cells toward the accumulation and functional augmentation of MYH10 (See **Discussion**).

Unlike the fact that CDC42EP4 positively regulates the association between GLAST and the septin complex in Bergman glia (Ageta-Ishihara et al., 2015), loss of CDC42EP4 did not alter the interaction between MYH10 and the septin complex in Bergmann glia (represented by SEPT4 in Fig. 4B) and neurons (represented by SEPT3 in Fig. 4C).

Accumulation of N-cadherin in *Cdc42ep4*$^{-/-}$ cerebellum

It has been established that submembranous actomyosin network physically and functionally interact with N-cadherin (Marrs et al., 2009; Bozdagi et al., 2010; Tanaka et al., 2012; Chazeau et al., 2015), and that homophilic interaction of N-cadherin mediates the adhesion between pre- and postsynaptic membranes at the outer borders and margins of an active zone of mature synapses (Uchida et al., 1996). Thus, we compared the status of N-cadherin in the pellet/supernatant fractions of *Cdc42ep4*$^{-/-}$ and WT cerebellar lysates by immunoblotting. The content of N-cadherin in the soluble fraction, but not in the insoluble fraction, was significantly higher in *Cdc42ep4*$^{-/-}$ cerebellar lysate (Fig. 4D). A previous study showed that several major proteins in the synaptic active zone are highly insoluble, while significant amount of N-cadherin, β-catenin, actin, and septins are partitioned to the soluble fraction under standard extraction conditions (Phillips et al., 2001). Together, all the above data indicate that the mild accumulations of N-cadherin and MYH10 account, at least in part, for the anomalous extension of nonactive synaptic contacts toward Purkinje cells in *Cdc42ep4*$^{-/-}$ cerebellum.

Discussion

We have demonstrated that mice that lack a Bergmann glia-selective scaffold protein CDC42EP4 harbor a set of anomalies in the most numerous glutamatergic tripartite synapses in the molecular layer of the cerebellar cortex. The morphological and functional anomalies in the perisynaptic component, *i.e.*, glial recession (this study) and inefficient glutamate clearance (Ageta-Ishihara et al., 2015), impinge on the neighboring neuronal components. The secondary augmentations of N-cadherin and MYH10 in neurons seem to underlie the extension of pre- and postsynaptic adhesion around the active zones, although the transcellular mechanism remains unclear.

MYH10, in conjunction with the actin cytoskeleton, not only generates tensile force for the proliferation and migration of neural precursor cells (Shenk et al., 2007), but also serves as a submembranous structural component that facilitates cell adhesion mediated by N-cadherin and other cell adhesion molecules (Uren et al., 2000; Ma et al., 2007; Tai et al., 2008). Given that N-cadherin is excluded from the active zones in mature synapses (Uchida et al., 1996), the concurrent augmentation of N-cadherin and MYH10 in cerebellar neurons of adult *Cdc42ep4*$^{-/-}$ mice suggests organization of superfluous synaptic contacts around the active zones.

The mode of glia-originated tripartite synapse anomalies found in *Cdc42ep4*$^{-/-}$ mice is regarded as a milder phenocopy of GLAST-null mice, where severe overflow of extracellular glutamate abolishes Bergmann glial coverage around pre- and postsynaptic components and developmental rewiring among cerebellar neurons (Miyazaki et al., 2017). Apart from the magnitude, the phenotypic similarity of *Cdc42ep4*$^{-/-}$ mice to GLAST-null mice and GLAST inhibitor-treated wildtype mice (Miyazaki et al., 2017) indicates that the inefficient glutamate clearance is the common transcellular mechanism linking the glial anomalies to the neuronal anomalies. Reciprocally, the phenotypic similarity to *Cdc42ep4*$^{-/-}$ mice predicts that adult GLAST-null mice harbor significant augmentations of N-cadherin and MYH10 in the cerebella. In either mutant, glutamate overflow around synapses would increase actin polymerization (Matsuzaki et al., 2004) and activity-dependent accumulation of β-catenin (Murase et al., 2002) in dendritic spines, which would synergistically promote MYH10 accumulation and N-cadherin-mediated adhesion of synaptic membranes (Takeichi and Abe, 2005; Rex et al., 2010; Friedman et al., 2015).

Despite the inefficient clearance and protracted retention of glutamate around parallel fiber-Purkinje cell synapses in *Cdc42ep4*$^{-/-}$ mice, the bulk content of glutamate in the whole cerebellar cortex was normal, which was also the case for some other amino acids (e.g., GABA, D-serine), monoamines (e.g., dopamine, noradrenaline), and neurotransmitter metabolites (Ageta-Ishihara et al., 2015). Since many of those molecules serve as

neurotransmitters, neuromodulators, and/or gliotransmitters (Perea et al., 2009), scrutiny of their local turnover might reveal unknown molecular pathways underlying the tripartite synapse anomalies.

Since Bergmann glial processes and Purkinje cell dendrites are finely intertwined, and MYH10 abounds in Purkinje cells but not in Bergmann glia, it is difficult to demonstrate the putative reduction of MYH10 in Bergmann glia, and the probable augmentation of MYH10 in Purkinje cells, in *Cdc42ep4*$^{-/-}$ cerebellum by immunofluorescence (Fig. 3E). This problem of quantification of MYH10 in each of the three synaptic compartments would be overcome by immunogold labeling and TEM observation. However, MYH10 antibodies applicable for immune-EM analysis is currently unavailable. Another remaining problem is whether the reduction of MYH10 in *Cdc42ep4*$^{-/-}$ Bergmann glia causes retraction of their perisynaptic processes, which could be tested by Bergmann glia-selective knockdown or inhibition of MYH10. Future studies addressing those and other outstanding problems with *Cdc42ep4*$^{-/-}$ and GLAST-null mice would provide unique clues to unravel the “three-body problem” of synapses.

Materials and Methods

Animal experiments

Animal experiments had been approved by institutional review committees and conducted in accordance with the regulations for the care and use of animals at Nagoya University, Hokkaido University and Niigata University.

Antibodies

We used original rabbit polyclonal antibodies for the following antigens: CDC42EP4 (Frontier Science AB_2571675, dilution 1:150) and SEPT4 (Ihara et al., 2007, 1:3000) as previously described, and one raised against and affinity purified with a synthetic oligopeptide Met^{1}-Lys^{17} from SEPT3 (this study). The sources and dilution of commercial antibodies are as follows: 3PGDH (Frontier Science, AB_2571653, 1 μg/ml), MYH10 (Covance PRB-445P, 1:2000), α-tubulin (Sigma T9026, 1:10000), GFP (Thermo A11122, 1:1000), β-actin (Sigma A5441, 1:1000), and MYH9 (Sigma M8064, 1:2000), N-cadherin (BD 610920, 1:250). For secondary antibodies, we used horseradish peroxidase- or Cy3-conjugated IgGs from mouse or rabbit (Cell signaling 7074 and 7076, Rockland 18-8816-31, Jackson ImmunoReseach711-165-152, 1:200).

Biochemical fractionation of brain tissues

The cerebellum from *Cdc42ep4*$^{-/-}$ and wild-type mice were dissected, weighed, homogenized by sonication in 3 ml/g of buffer A (10 mM Tris-HCl pH 7.6, 0.15 M NaCl, 1% Triton X-100, and protease inhibitors). The supernatant after centrifugation at 20,400 x g at 4°C for 0.5 h was labeled as soluble fraction. The washed pellet was dissolved with sonication in buffer B (3 ml/g; 0.1 M Tris-HCl pH 6.8, 4% SDS, 20% glycerol), whose final volume was adjusted to that of the cognate soluble fraction, and was labeled as pellet/insoluble fraction. After measuring protein concentration with a BCA method, each sample was mixed with an equal amount of 2x sample buffer (0.1 M Tris-HCl pH 6.8, 4% SDS, 20% glycerol, 20% 2-mercaptoethanol and 0.01% bromophenol blue) and incubated for 0.5 h at RT.

Immunoblotting and densitometry

The protein content in each fraction was measured and incubated with Laemmli buffer. Each soluble fraction was loaded with the equivalent amount of the cognate pellet/insoluble fraction in an adjacent lane of 10% polyacrylamide gel. Polypeptides resolved by electrophoresis were transferred onto reinforced PVDF membranes (Millipore, IPVH00010) using a semidry,

discontinuous buffer method (Parajuli et al., 2016). The membranes were blocked with 5% skim milk in Tris-buffered saline (TBS; 0.1 M Tris-HCl pH 7.4, 150 mM NaCl) containing 0.05% Tween-20 and incubated serially with the primary antibodies and anti-rabbit or -mouse IgG conjugated with horseradish peroxidase (Jackson ImmunoResearch). After extensive wash with TBS plus 0.05% Tween-20, chemiluminescence detection and densitometry were conducted with ECL-Plus reagent (PerkinElmer) and an image analyzer LAS4000mini with MultiGauge software (GE).

Immunofluorescence, and fluorescence and electron microscopy

Mouse brains were dissected after deep anesthesia with sodium pentobarbital (0.1 mg/g, i.p.) with transcardial perfusion with 0.01 M phosphate-buffered saline (PBS), then with with 4% paraformaldehyde in 0.1 M phosphate buffer (PB) at pH 7.2 for IF, or with 2% paraformaldehyde/2% glutaraldehyde in PB for TEM. The brains excised from the skull were immersed in the same fixative for 3 days, then 4-μm-thick paraffin sections for IF (for 3PDGH, MYH10, and SEPT4) were made with a sliding microtome (SM1000R, Leica) and used in IF, or 50-μm-thick sections for TEM were made with a microslicer (VT1000S, Leica), and subjected to free-floating incubation. For IF, slices were incubated with 10% normal donkey serum for 20 min, a mixture of primary antibodies overnight, and a mixture of Alexa 488- or Cy3-labeled species-specific secondary antibodies for 2 h. Fluorescence imaging was conducted using scanning laser confocal microscopes IX81/FV1000 (Olympus) with a 40×, NA 1.0 objective lens and LSM-780 (Zeiss) with 63×, NA 1.4 objective lenses. For TEM, ultrathin sections were mounted on grids and stained with 2% uranyl acetate for 20 min, and observed with a TEM (H-7100, Hitachi) as described previously (Fukaya et al., 2000; Abe et al., 2004).

Cell culture and spreading

COS-7 cells (monkey kidney-derived cell line) were grown in Dulbecco's modified Eagle medium containing 10% fetal bovine serum (FBS), and co-transfected with GFP or GFP-CDC42EP4 and TagRFP using Lipofectamine 2000 (Thermo Fisher). After 24 h, cells were collected using trypsin/0.25% EDTA, allowed to spread for 1 h, then fixed with 4% PFA/PBS for 15 min. Serial confocal images were acquired with a 63x objective lens (NA 1.4) on the laser microscope LSM-780. Cell area was measured using ImageJ-based software, Fiji (NIH).

Statistical analysis

Quantitative data were expressed as mean ± s.e.m. For statistical analyses, either two tailed t-test

or Kolmogorov-Smirnov test were applied using Prism 6.03 (GraphPad Software). p values represent the effects of genotype.

Acknowledgements

This work was supported in part by Grants-in-Aid for Scientific Research on Innovative Areas ("Glia Assembly", "Adaptive Circuit Shift" and "Microendophenotype of psychiatric disorders"), and supports from Comprehensive Brain Science Network and Advanced Bioimaging Support (ABiS) from the Ministry of Education, Science, Sports and Culture of Japan.

Authors' contributions

MY, MA, and KS established *Cdc42ep4*$^{-/-}$ line. KK and MW conducted histological and TEM analysis. NA-I conducted the biochemical and cell biological analyses. MK designed the experiment and wrote the manuscript. All authors read and approved the manuscript.

References

Abe, M., Fukaya, M., Yagi, T., Mishina, M., Watanabe, M., Sakimura, K., 2004. NMDA receptor GluRepsilon/NR2 subunits are essential for postsynaptic localization and protein stability of GluRzeta1/NR1 subunit. J Neurosci 24, 7292-7304.

Ageta-Ishihara, N., Yamazaki, M., Konno, K., Nakayama, H., Abe, M., Hashimoto, K., Nishioka, T., Kaibuchi, K., Hattori, S., Miyakawa, T., Tanaka, K., Huda, F., Hirai, H., Hashimoto, K., Watanabe, M., Sakimura, K., Kinoshita, M., 2015. A CDC42EP4/septin-based perisynaptic glial scaffold facilitates glutamate clearance. Nat Commun 6, 10090.

Altman, J. and Bayer, S.A., 1997. Development of the Cerebellar System: In Relation to Its Evolution, Structure, and Functions. CRC Press

Araque, A., Parpura, V., Sanzgiri, R.P., Haydon, P.G., 1999. Tripartite synapses: glia, the unacknowledged partner. Trends Neurosci 22, 208-215.

Belvindrah, R., Nalbant, P., Ding, S., Wu, C., Bokoch, G.M., Muller, U., 2006. Integrin-linked kinase regulates Bergmann glial differentiation during cerebellar development. Mol Cell Neurosci 33, 109-125.

Betapudi, V., 2014. Life without double-headed non-muscle myosin II motor proteins. Front Chem 2, 45.

Betapudi, V., Licate, L.S., Egelhoff, T.T., 2006. Distinct roles of nonmuscle myosin II isoforms in the regulation of MDA-MB-231 breast cancer cell spreading and migration. Cancer Res 66, 4725-4733.

Bozdagi, O., Wang, X.B., Nikitczuk, J.S., Anderson, T.R., Bloss, E.B., Radice, G.L., Zhou, Q., Benson, D.L., Huntley, G.W., 2010. Persistence of coordinated long-term potentiation and dendritic spine enlargement at mature hippocampal CA1 synapses requires N-cadherin. J Neurosci 30, 9984-9989.

Cai, Y., Biais, N., Giannone, G., Tanase, M., Jiang, G., Hofman, J.M., Wiggins, C.H., Silberzan, P., Buguin, A., Ladoux, B., Sheetz, M.P., 2006. Nonmuscle myosin IIA-dependent force inhibits cell spreading and drives F-actin flow. Biophys J 91, 3907-3920.

Calvo, F., Ranftl, R., Hooper, S., Farrugia, A.J., Moeendarbary, E., Bruckbauer, A., Batista, F., Charras, G., Sahai, E., 2015. Cdc42EP3/BORG2 and Septin Network Enables Mechano-transduction and the Emergence of Cancer-Associated Fibroblasts. Cell Rep 13, 2699-2714.

Chazeau, A., Garcia, M., Czondor, K., Perrais, D., Tessier, B., Giannone, G., Thoumine, O., 2015. Mechanical coupling between transsynaptic N-cadherin adhesions and actin flow stabilizes dendritic spines. Mol Biol Cell 26, 859-873.

Chen, Y., Fu, A.K., Ip, N.Y., 2008. Bidirectional signaling of ErbB and Eph receptors at synapses. Neuron Glia Biol 4, 211-221.

Friedman, L.G., Benson, D.L., Huntley, G.W., 2015. Cadherin-based transsynaptic networks in establishing and modifying neural connectivity. Curr Top Dev Biol 112, 415-465.

Fukaya., M., Watanabe, M., 2000. Improved immunohistochemical detection of postsynaptically located PSD-95/SAP90 protein family by protease section pretreatment: a study in the adult mouse brain. J Comp Neurol 426, 572-586.

Garrett, A.M., Weiner, J.A., 2009. Control of CNS synapse development by γ-protocadherin-mediated astrocyte-neuron contact. J Neurosci 29, 11723-11731.

Hagiwara, A., Tanaka, Y., Hikawa, R., Morone, N., Kusumi, A., Kimura, H., Kinoshita, M., 2011. Submembranous septins as relatively stable components of actin-based membrane skeleton. Cytoskeleton (Hoboken) 68, 512-525.

Halassa, M.M., Fellin, T., Haydon, P.G., 2007. The tripartite synapse: roles for gliotransmission in health and disease. Trends Mol Med 13, 54-63.

Ihara, M., Yamasaki, N., Hagiwara, A., Tanigaki, A., Kitano, A., Hikawa, R., Tomimoto, H., Noda, M., Takanashi, M., Mori, H., Hattori, N., Miyakawa, T., Kinoshita, M., 2007. Sept4, a

component of presynaptic scaffold and Lewy bodies, is required for the suppression of alpha-synuclein neurotoxicity. Neuron 53, 519-33.

Iino, M., Goto, K., Kakegawa, W., Okado, H., Sudo, M., Ishiuchi, S., Miwa, A., Takayasu, Y., Saito, I., Tsuzuki, K., Ozawa, S., 2001. Glia-synapse interaction through Ca2+-permeable AMPA receptors in Bergmann glia. Science 292, 926-929.

Joberty, G., Perlungher, R.R., Macara, I.G., 1999. The Borgs, a new family of Cdc42 and TC10 GTPase-interacting proteins. Mol Cell Biol 19, 6585-6597.

Joberty, G., Perlungher, R.R., Sheffield, P.J., Kinoshita, M., Noda, M., Haystead, T., Macara, I.G., 2001. Borg proteins control septin organization and are negatively regulated by Cdc42. Nat Cell Biol 3, 861-866.

Joo, E., Surka, M.C., Trimble, W.S., 2007. Mammalian SEPT2 is required for scaffolding nonmuscle myosin II and its kinases. Dev Cell 13, 677-90.

Kinoshita, N., Kimura, K., Matsumoto, N., Watanabe, M., Fukaya, M., Ide, C., 2004. Mammalian septin Sept2 modulates the activity of GLAST, a glutamate transporter in astrocytes. Genes Cells 9, 1-14.

Kolega, J., 2003. Asymmetric distribution of myosin IIB in migrating endothelial cells is regulated by a rho-dependent kinase and contributes to tail retraction. Mol Biol Cell 14, 4745-4757.

Liu, Z., Ho, C.H., Grinnell, F., 2014a. The different roles of myosin IIA and myosin IIB in contraction of 3D collagen matrices by human fibroblasts. Exp Cell Res 326, 295-306.

Liu, Z., Vong, Q.P., Liu, C., Zheng, Y., 2014b. Borg5 is required for angiogenesis by regulating persistent directional migration of the cardiac microvascular endothelial cells. Mol Biol Cell 25, 841-851.

Lo, C.M., Buxton, D.B., Chua, G.C., Dembo, M., Adelstein, R.S., Wang, Y.L., 2004. Nonmuscle myosin IIb is involved in the guidance of fibroblast migration. Mol Biol Cell 15, 982-989.

Ma, X., Bao, J., Adelstein, R.S., 2007. Loss of cell adhesion causes hydrocephalus in nonmuscle myosin II-B-ablated and mutated mice. Mol Biol Cell 18, 2305-2312.

Ma, X., Kawamoto, S., Uribe, J., Adelstein, R.S., 2006. Function of the neuron-specific alternatively spliced isoforms of nonmuscle myosin II-B during mouse brain development. Mol Biol Cell 17, 2138-2149.

Marrs, G.S., Theisen, C.S., Bruses, J.L., 2009. N-cadherin modulates voltage activated calcium influx via RhoA, p120-catenin, and myosin-actin interaction. Mol Cell Neurosci 40, 390-400.Matsuzaki, M., Honkura, N., Ellis-Davies, G.C., Kasai, H., 2004. Structural basis of long-term potentiation in single dendritic spines. Nature 429, 761-6.

Miyazaki, T., Watanabe, M., Yamagishi, A., Takahashi, M., 2000. B2 exon splicing of nonmuscle myosin heavy chain IIB is differently regulated in developing and adult rat brain. Neurosci Res 37, 299-306.

Miyazaki, T., Yamasaki, M., Hashimoto, K., Kohda, K., Yuzaki, M., Shimamoto, K., Tanaka, K., Kano, M., Watanabe, M., 2017. Glutamate transporter GLAST controls synaptic wrapping by Bergmann glia and ensures proper wiring of Purkinje cells. Proc Natl Acad Sci U S A, 114, 7438-7443.

Moncman, C.L., Rindt, H., Robbins, J., Winkelmann, D.A., 1993. Segregated assembly of muscle myosin expressed in nonmuscle cells. Mol Biol Cell 4, 1051-1067.

Murase, S., Mosser, E., Schuman, E.M., 2002. Depolarization drives beta-Catenin into neuronal spines promoting changes in synaptic structure and function. Neuron 35, 91-105.

Parajuli, L.K., Ageta-Ishihara, N., Ageta, H., Fukazawa, Y., Kinoshita, M., 2016. Methods for immunoblot detection and electron microscopic localization of septin subunits in mammalian nervous systems. Methods Cell Biol 136, 285-294.

Perea, G., Navarrete, M., Araque, A., 2009. Tripartite synapses: astrocytes process and control synaptic information. Trends Neurosci 32, 421-431.

Phillips, G.R., Huang, J.K., Wang, Y., Tanaka, H., Shapiro, L., Zhang, W., Shan, W.S., Arndt, K., Frank, M., Gordon, R.E., Gawinowicz, M.A., Zhao, Y., Colman, D.R., 2001. The presynaptic particle web: ultrastructure, composition, dissolution, and reconstitution. Neuron 32, 63-77.

Rex, C., Gavin, C.F., Rubio, M.D., Kramar, E.A., Chen, L.Y., Jia, Y., Huganir, R.L., Muzyczka, N., Gall, C.M., Miller, C.A., Lynch, G., Rumbaugh, G., 2010. Myosin IIB regulates actin dynamics during synaptic plasticity and memory formation. Neuron 67, 603–617.

Schenk, J., Wilsch-Brauninger, M., Calegari, F., Huttner, W.B., 2009. Myosin II is required for interkinetic nuclear migration of neural progenitors. Proc Natl Acad Sci U S A 106, 16487-16492.

Sellers, J.R., 2000. Myosins: a diverse superfamily. Biochim Biophys Acta 1496, 3-22.

Tai, C.Y., Kim, S.A., Schuman, E.M., 2008. Cadherins and synaptic plasticity. Curr Opin Cell Biol 20, 567-575.

Takeichi, M., Abe, K., 2005. Synaptic contact dynamics controlled by cadherin and catenins. Trends Cell Biol 15, 216-221.

Tanaka, H., Takafuji, K., Taguchi, A., Wiriyasermkul, P., Ohgaki, R., Nagamori, S., Suh, P.G., Kanai, Y., 2012. Linkage of N-cadherin to multiple cytoskeletal elements revealed by a proteomic approach in hippocampal neurons. Neurochem Int 61, 240-250.

Uchida, N., Honjo, Y., Johnson, K.R., Wheelock, M.J., Takeichi, M., 1996. The catenin/cadherin adhesion system is localized in synaptic junctions bordering transmitter release zones. J Cell Biol 135, 767-779.

Uren, D., Hwang, H.K., Hara, Y., Takeda, K., Kawamoto, S., Tullio, A.N., Yu, Z.X., Ferrans, V.J., Tresser, N., Grinberg, A., Preston, Y.A., Adelstein, R.S., 2000. Gene dosage affects the cardiac and brain phenotype in nonmuscle myosin II-B-depleted mice. J Clin Invest 105, 663-671.

Vicente-Manzanares, M., Ma, X., Adelstein, R.S., Horwitz, A.R., 2009. Non-muscle myosin II takes centre stage in cell adhesion and migration. Nat Rev Mol Cell Biol 10, 778-790.

Watanabe, M., 2002. Glial processes are glued to synapses via Ca^{2+}-permeable glutamate receptors. Trends Neurosci 25, 5-6.

Yamada, K., Fukaya, M., Shibata, T., Kurihara, H., Tanaka, K., Inoue, Y., Watanabe, M., 2000. Dynamic transformation of Bergmann glial fibers proceeds in correlation with dendritic outgrowth and synapse formation of cerebellar Purkinje cells. J Comp Neurol 418, 106-120.

Zhao, X., Rotenberg, S.A., 2014. Phosphorylation of Cdc42 effector protein-4 (CEP4) by protein kinase C promotes motility of human breast cells. J Biol Chem 289, 25844-25854.

Figure Legends

Figure 1. Anomalous configuration of tripartite synapses in the cerebellar cortex of *Cdc42ep4*$^{-/-}$ mice

(A-D) Immunofluorescence for a Bergmann glia marker 3-phosphoglycerate dehydrogenase (3PDGH) on parasagittal cerebellar sections of adult male *Cdc42ep4*$^{fl/fl}$ (WT; A, B) and *Cdc42ep4*$^{-/-}$ (KO; C, D) littermates. Cdc42ep4 KO mice are normal in somatic positioning of Bergmann glia around Purkinje cell somata and in palisade-like alignment of Bergmann fibers in the molecular layer. ML, molecular layer; PCL, Purkinje cell layer. Scale bar, 20 μm (A, C) or 5 μm (B, D).

(E, F) Representative TEM images of tripartite synapses in the cerebellar molecular layer of WT (E) and KO (F) littermates. The length the active zone, which is equivalent to that of PSD (the distance between a pair of black arrowheads), was comparable by genotype (Ageta-Ishihara et al., 2015). However, the distance measured from an edge of a PSD to the nearest tip of Bergmann glial membrane (a pair of red arrowheads) appeared to extend in KO cerebella (Fig. 1F). PF: parallel fiber terminal or bouton. Sp: dendritic spine of Purkinje cell. Terminal lamellae of Bergmann glial processes are tinted. Scale bar, 200 nm.

(G) Cumulative histogram of PSD edge-glial tip distance, showing a statistically significant extension in KO by the right-shift of the curve (n=92, 92 synapses from WT and KO littermates, $p= 7.00 \times 10^{-6}$ by Kolmogorov-Smirnov test).

(H) The PSD edge-glial tip distance, which corresponds to the nonactive synaptic contact, was significantly greater in KO than in WT (152.4 ± 14.7 vs. 58.9 ± 8.18 nm; n=90, 86 synapses; p= 0.0001 by Mann-Whitney U test). Data represented as mean ± s.e.m.

Figure 2. Expression of CDC42EP4 in heterologous cells promotes spreading and accumulation of MYH10 in insoluble fraction

(A) (top) Representative fluorescence images of COS-7 cells co-expressing either GFP or GFP-CDC42EP4, with a volume marker TagRFP. Each image is a projection of 0.5 μm-thick serial optical sections acquired at 1 h after replating, 25 h after transfection. Unlike GFP and TagRFP, GFP-CDC42EP4 was distributed selectively in the cytoplasm (*i.e.*, excluded from the nucleus). Scale bar, 10 μm.

(bottom) Quantification of cell area in the spreading assay. GFP-CDC42EP4-expressing cells spread significantly more widely than GFP-expressing control cells (n=10, p= 0.0068 by Student's t test). Data represented as mean ± s.e.m.

(B) Results from the supernatant/pellet assay using cell lysates as in (A).
(top) Representative immunoblot for endogenous MYH10 in the soluble (Sup for supernatant) and the insoluble (pellet) fractions. In COS-7 cells expressing GFP-CDC42EP4, significantly more MYH10 is partitioned to the insoluble fraction than those expressing GFP alone.
(bottom) Quantification of MYH10 in triplicated experiments using α-tubulin as a loading control. A significant augmentation of MYH10 was observed in the insoluble fraction of GFP-CDC42EP4-expressing cells (x ~2.6; n=3, p= 0.017 by Student's t test) without reduction in the soluble fraction, indicating an increment in the total amount of MYH10 in cells. ~~These data from heterologous cells indicate positive effects of GFP-CDC42EP4 on the activity and/or stability of MYH10.~~ Data represented as mean ± s.e.m.

Figure 3. Selective augmentation of MYH10 in postdevelopmental *Cdc42ep4*$^{-/-}$ cerebellum
(A) Representative quantitative immunoblot for MYH10 in the supernatant/pellet assay of cerebellar lysate from adult (3.5-8 months of age) male *Cdc42ep4*$^{fl/fl}$ (WT) and *Cdc42ep4*$^{-/-}$ (KO) littermates, conducted as in Fig. 2B. MYH10 significantly increased (x ~1.5) in the insoluble fraction in KO (triplicated experiments, n=3, 3, p= 0.012 by Student's t test), with a trend of increase in the soluble fraction (p= 0.13). Data represented as mean ± s.e.m.
(B-C) MYH9 (B) and β-actin (C) analyzed likewise in the same set of samples as in (A) were comparable between WT and KO (triplicated experiments, n=3, 3, p= 0.38, 0.49, 0.82, and 0.13 by Student's t test). Data represented as mean ± s.e.m.
(D) MYH10 was not augmented in the cerebella of 4-week-old *Cdc42ep4*$^{-/-}$ pups (n=3, 3, p= 0.23, and 0.8 by Student's t test) ~~indicating~~ showing that genetic loss of CDC42EP4 causes selective augmentation of MYH10 in the cerebellum after maturity. Data represented as mean ± s.e.m.
(E) Immunofluorescence for MYH10 and a Bergmann glia-selective septin subunit SEPT4 on parasagittal cerebellar sections of adult male WT and KO littermates. MYH10 highlighted Purkinje cell somata and dendrites against weaker staining of neuropil and glial processes, which were comparable by genotype. ~~These data indicate that Purkinje cells are the principal source of MYH10 in the cerebellum, and that the augmentation of MYH10 in KO cerebella is not attributed to Bergmann glia.~~ Note that SEPT4 abounds in peripheral lamellar processes of Bergmann glia in contrast to 3PDGH (Fig. 1A). Scale bar, 20 μm.

Figure 4. The major source of MYH10 in the cerebellum is Purkinje cells
(A-C) Representative sets of images from immunoprecipitation-coupled immunoblot (IP-IB) assay for MYH10 using antibodies against CDC42EP4 (A), SEPT4 (B), and SEPT3 (C). MYH10

was barely detected in WT cerebellar lysates pulled down with antibodies for Bergmann glia-selective proteins, CDC42EP4 (A) and SEPT4 (B). In contrast, MYH10 was co-immunoprecipitated with a neuron-selective septin subunit SEPT3 in the presence or absence of CDC42EP4 (C). These data also indicate that the loss of CDC42EP4 does not alter MYH10-septin interaction in Bergmann glia and neurons, whereas it attenuates GLAST-septin interaction in Bergmann glia (Ageta-Ishihara et al., 2015).

(D) Results from the supernatant/pellet assay for endogenous N-cadherin using cerebellar lysates from WT and KO mice.

(top) Representative immunoblot for endogenous N-cadherin in the soluble and the insoluble fractions.

(bottom) Quantification in triplicated experiments using α-tubulin as a loading control. A significant increment of N-cadherin (the major band of 135kDa) was observed in the soluble fraction of the cerebella from KO mice (x ~1.4; n=3, 3, p= 0.04 by Student's t test) without reduction in the insoluble fraction, indicating an increment in the total amount of N-cadherin in cells. Data represented as mean ± s.e.m.

Supplemental Figure-S1

A gallery of Bergmann glia visualized by a Golgi impregnation method in WT and KO cerebella. Scale bars, 20 μm and 5 μm. See Miyazaki et al., 2017 for methods.

Cdc42ep4$^{fl/fl}$ (WT)

Cdc42ep4$^{-/-}$ (KO)

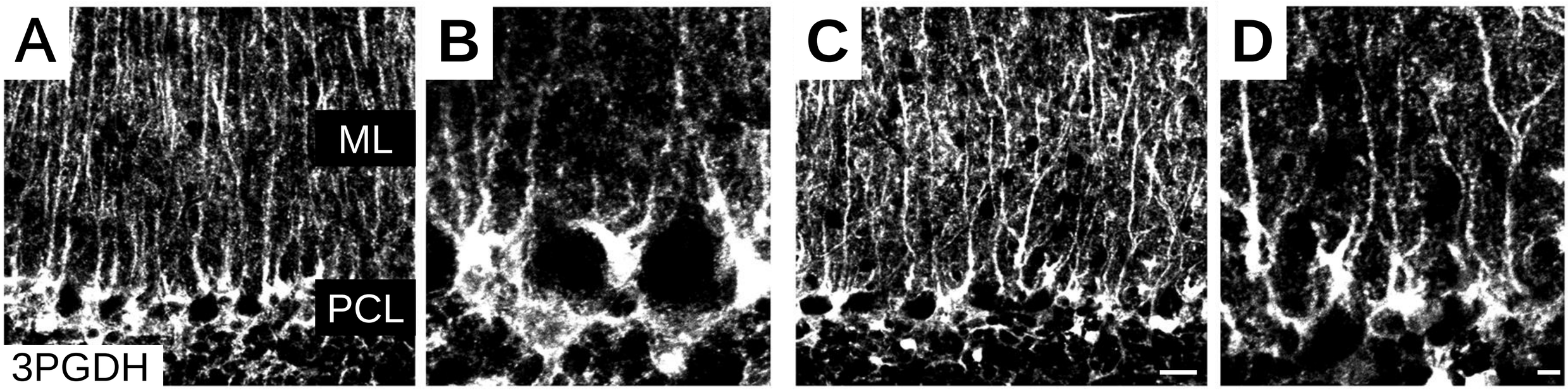

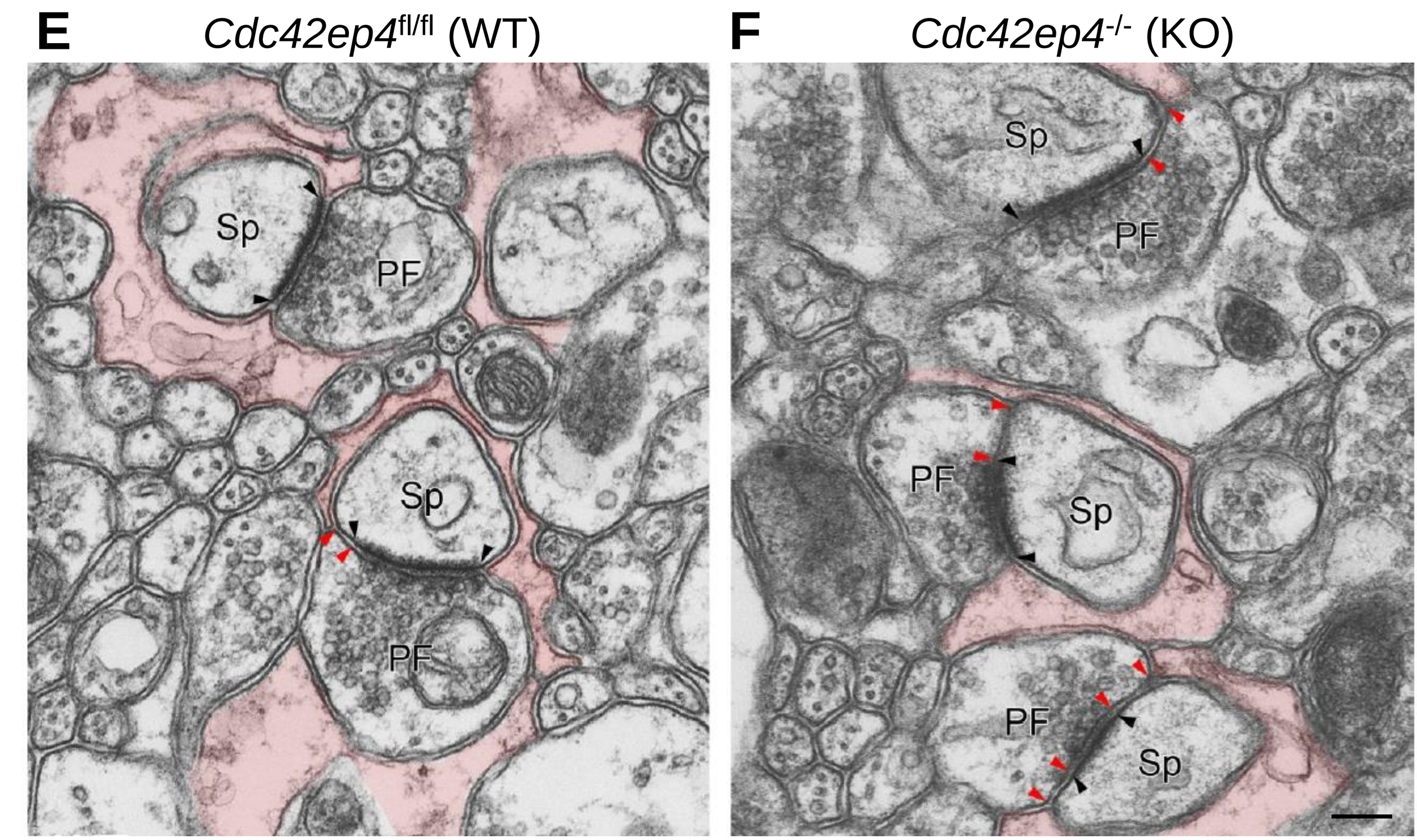

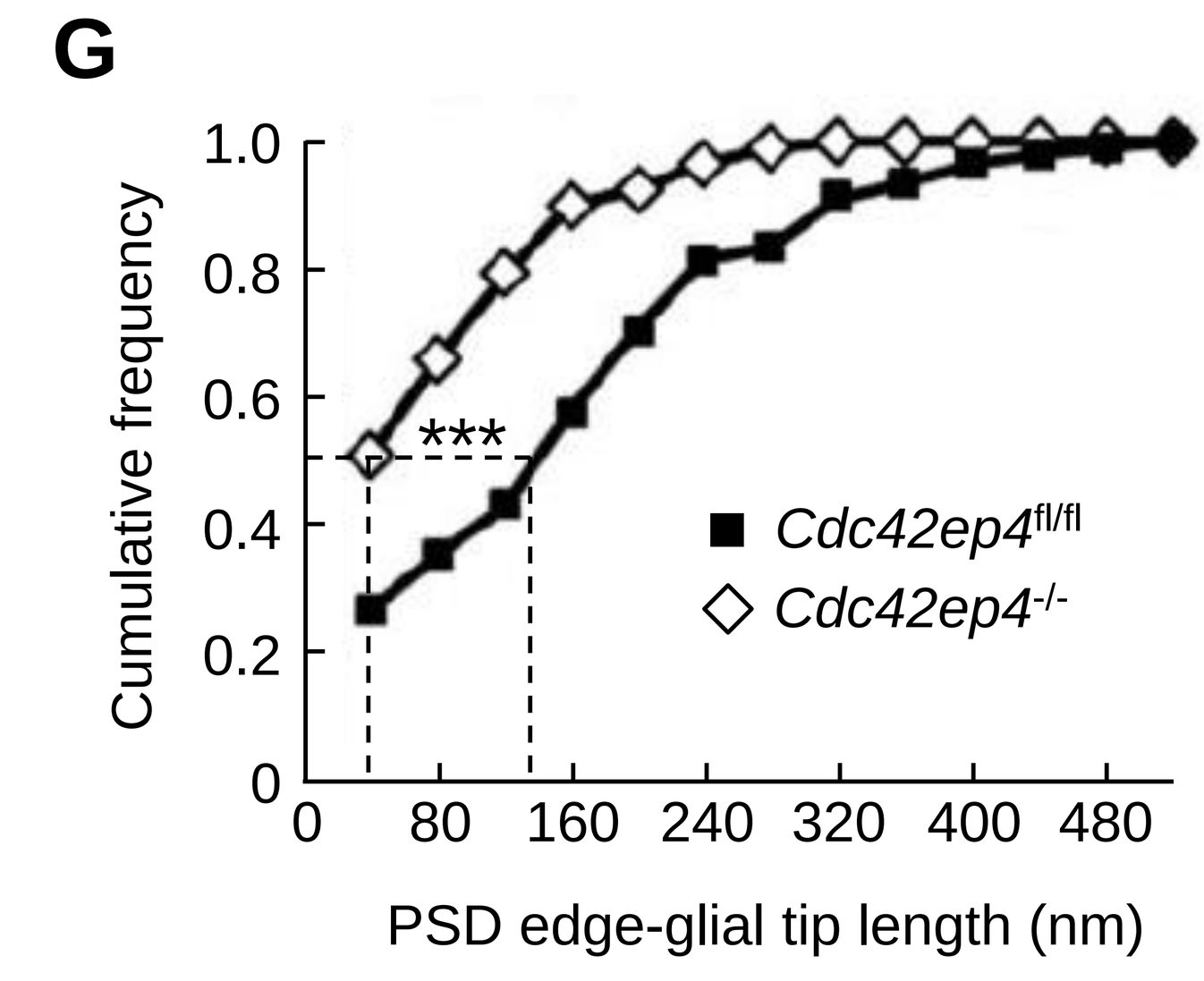

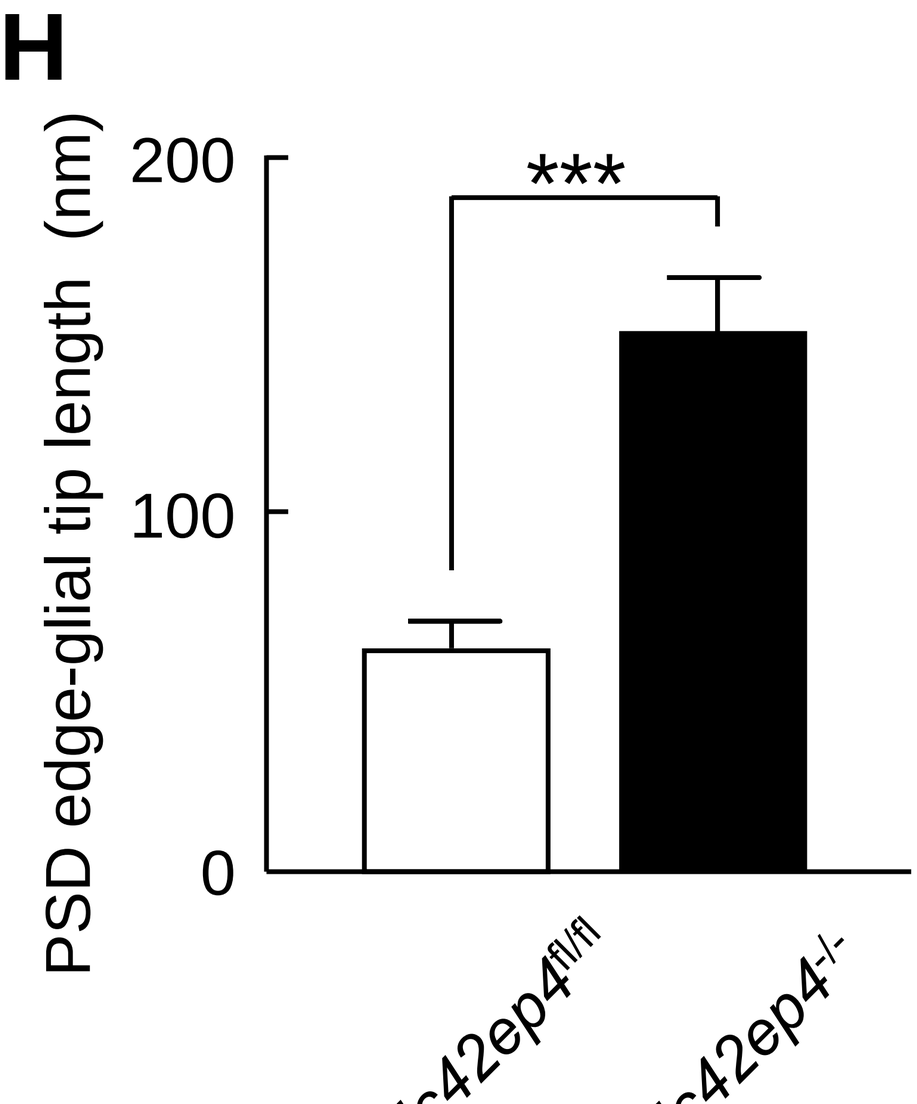

A

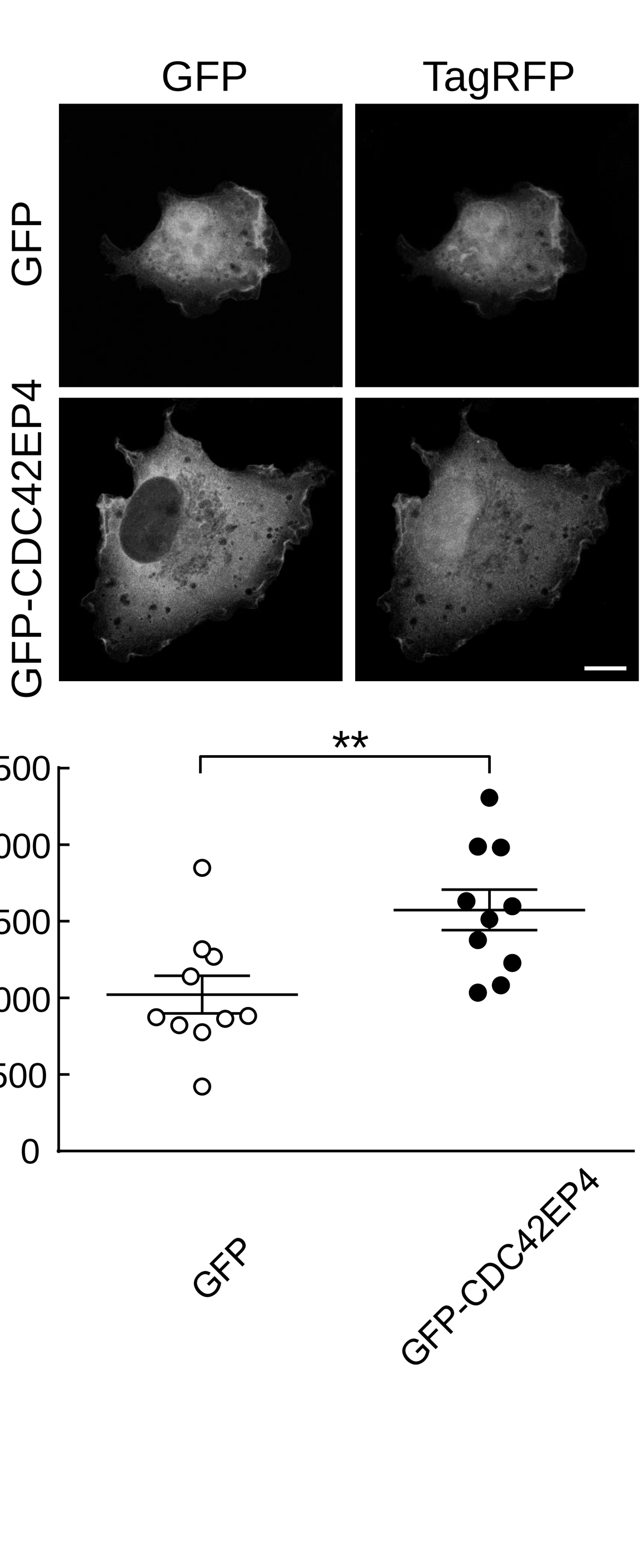
GFP
TagRFP
GFP
GFP-CDC42EP4

**
Cell area (μm²)
2500
2000
1500
1000
500
0
GFP
GFP-CDC42EP4

B

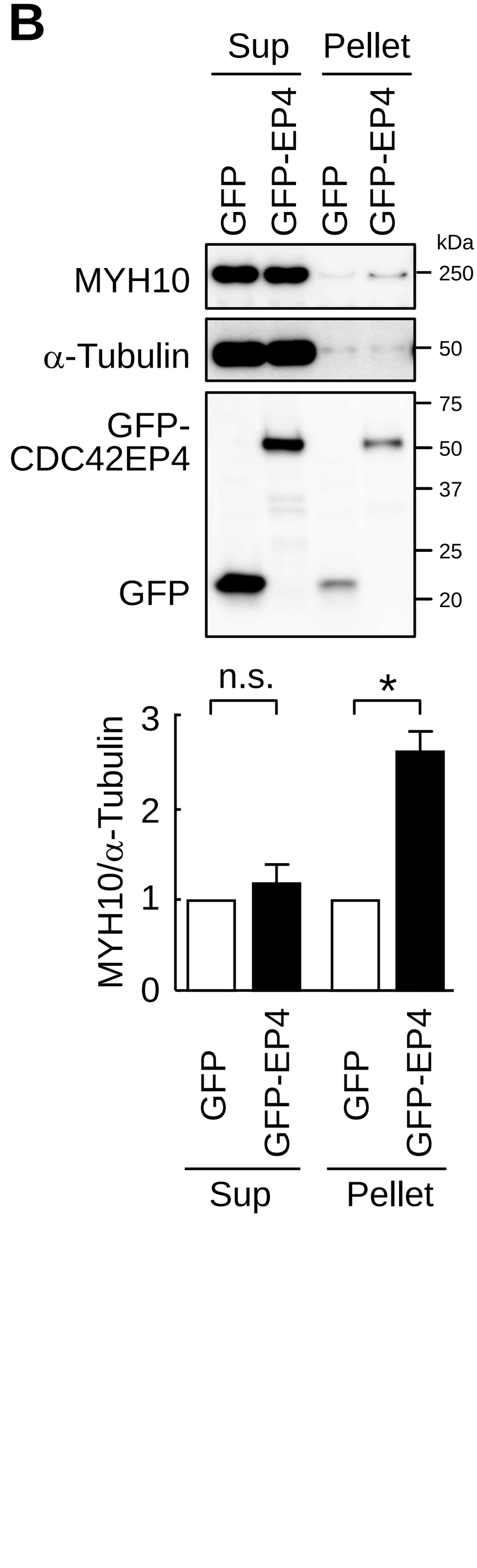
Sup
Pellet
GFP
GFP-EP4
GFP
GFP-EP4
kDa
MYH10
250
α-Tubulin
50
GFP-
CDC42EP4
75
50
37
25
GFP
20

n.s.
*
MYH10/α-Tubulin
3
2
1
0
GFP
GFP-EP4
GFP
GFP-EP4
Sup
Pellet

Figure- 3

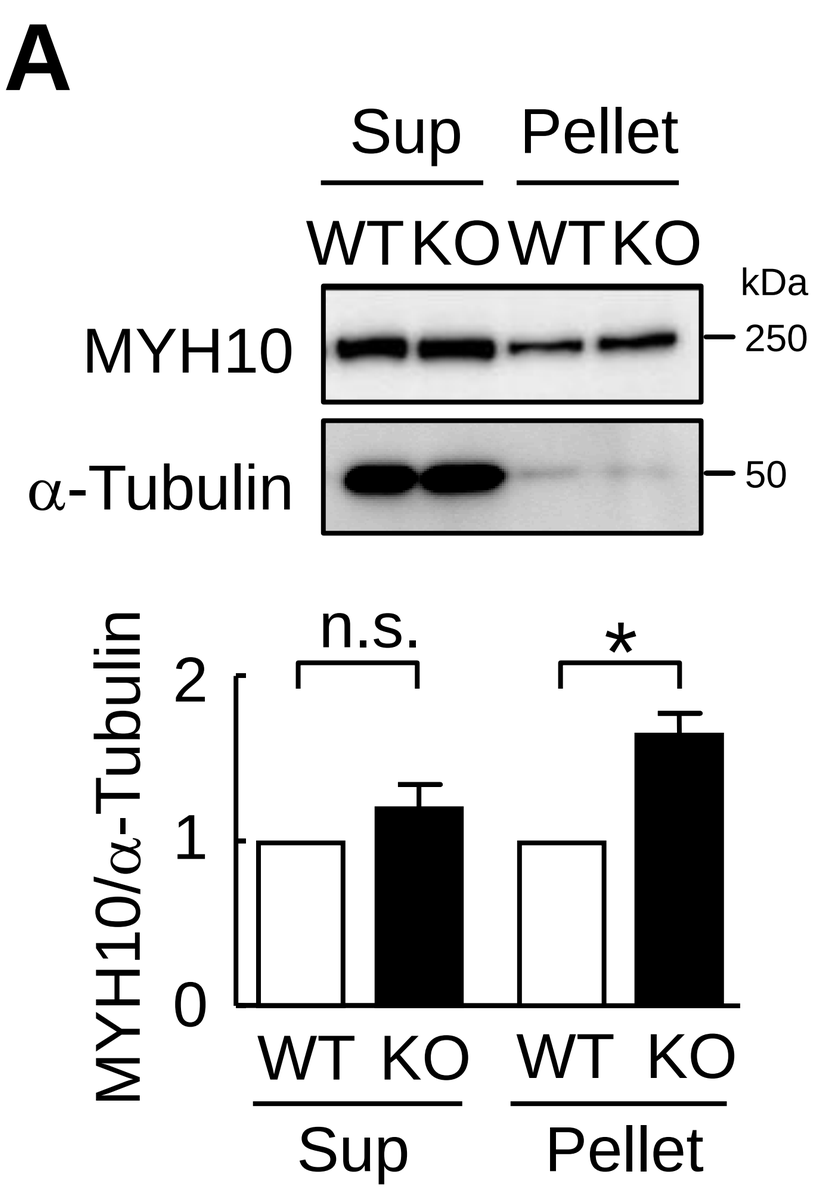
A
Sup
Pellet
WT KO WT KO
kDa
MYH10
250
α-Tubulin
50
MYH10/α-Tubulin
2
1
0
n.s.
*
WT KO
WT KO
Sup
Pellet

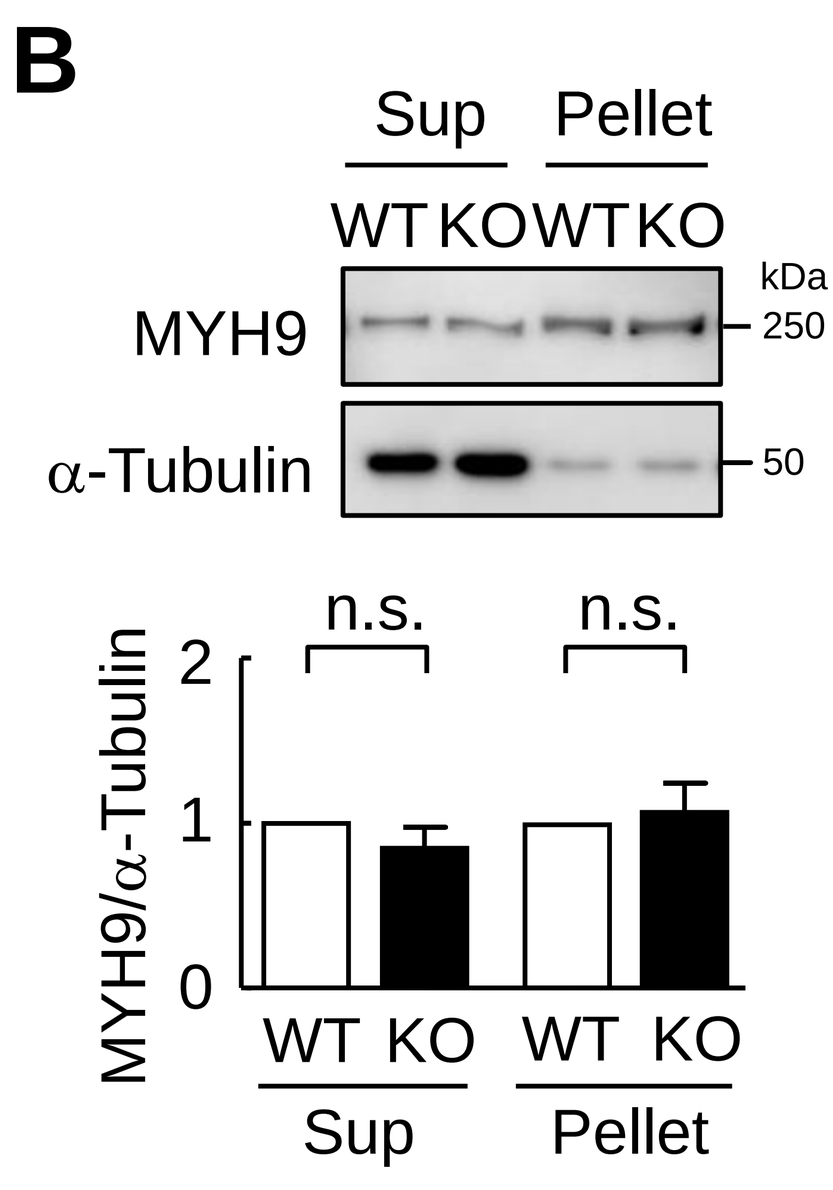
B
Sup
Pellet
WT KO WT KO
kDa
MYH9
250
α-Tubulin
50
MYH9/α-Tubulin
2
1
0
n.s.
n.s.
WT KO
WT KO
Sup
Pellet

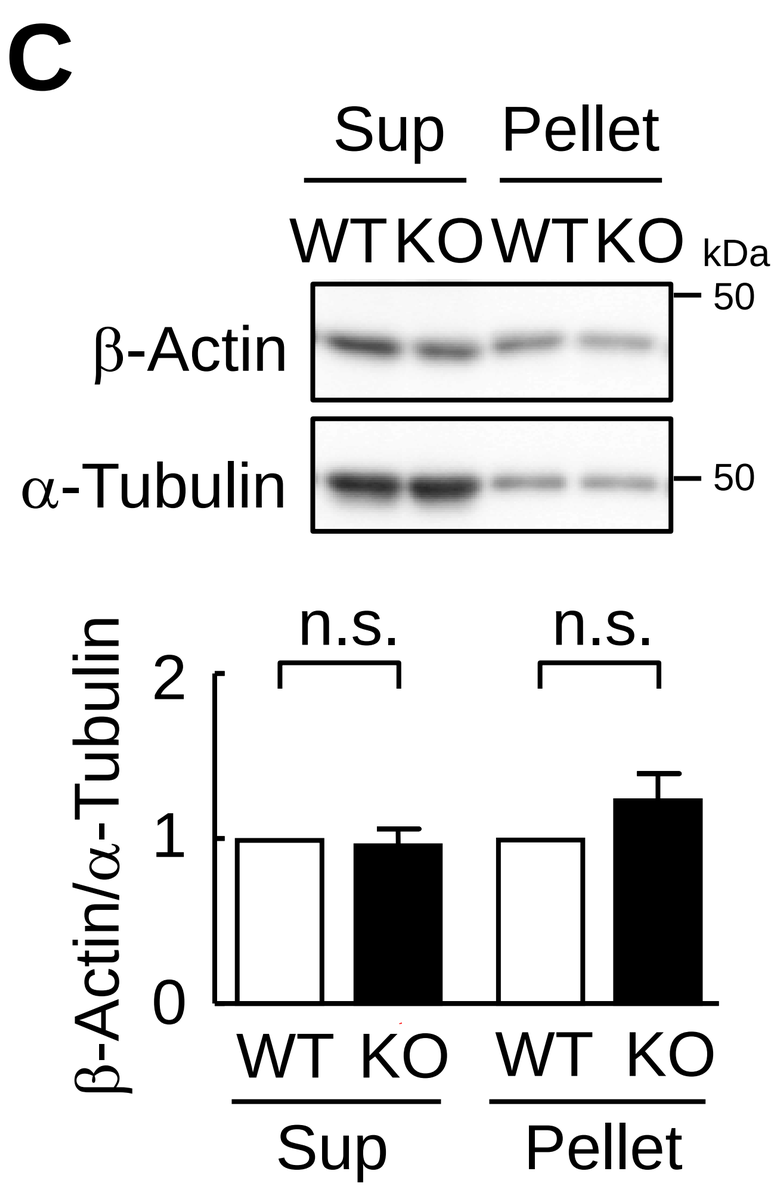
C
Sup
Pellet
WT KO WT KO
kDa
β-Actin
50
α-Tubulin
50
β-Actin/α-Tubulin
2
1
0
n.s.
n.s.
WT KO
WT KO
Sup
Pellet

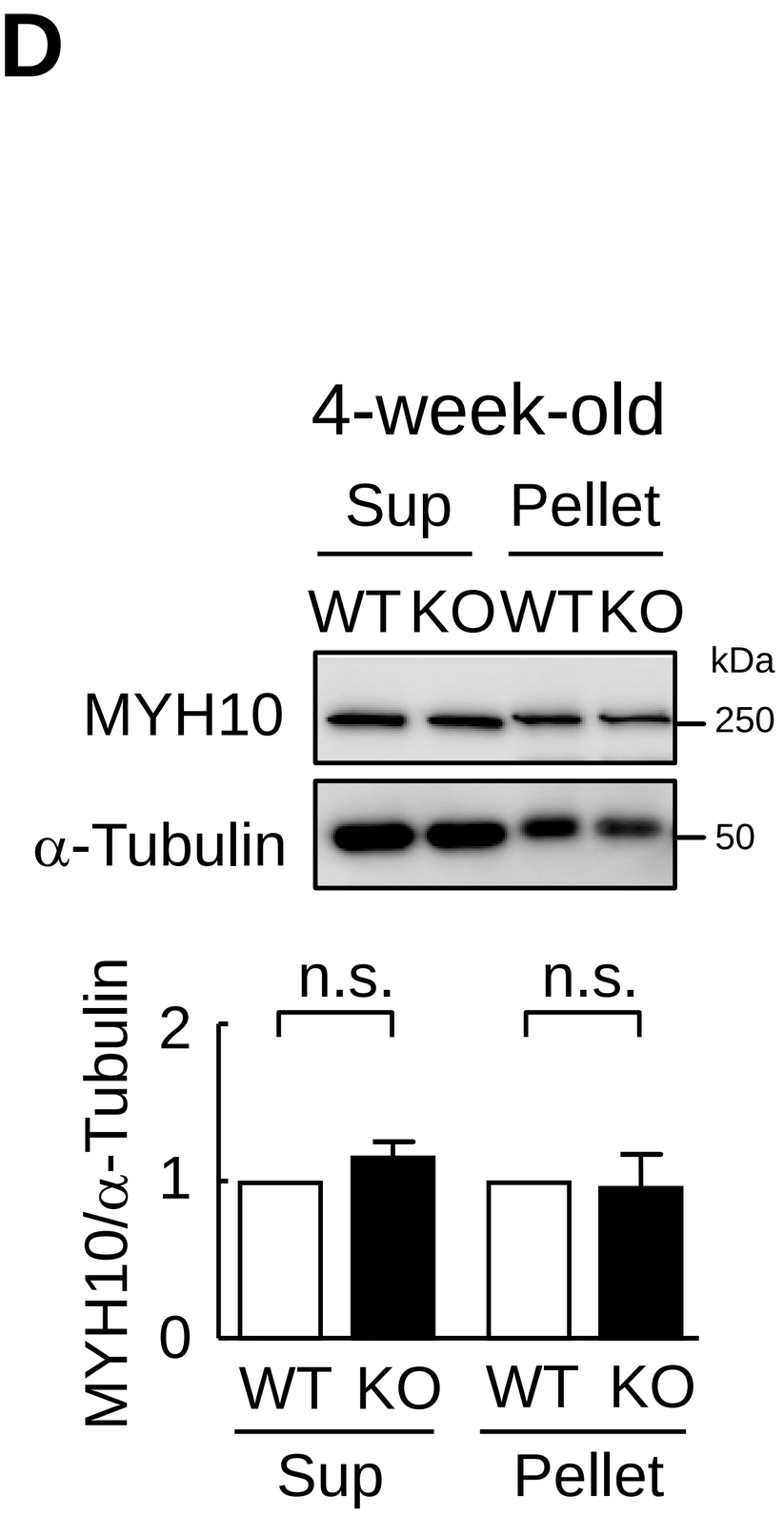
D
4-week-old
Sup
Pellet
WT KO WT KO
kDa
MYH10
250
α-Tubulin
50
MYH10/α-Tubulin
2
1
0
n.s.
n.s.
WT KO
WT KO
Sup
Pellet

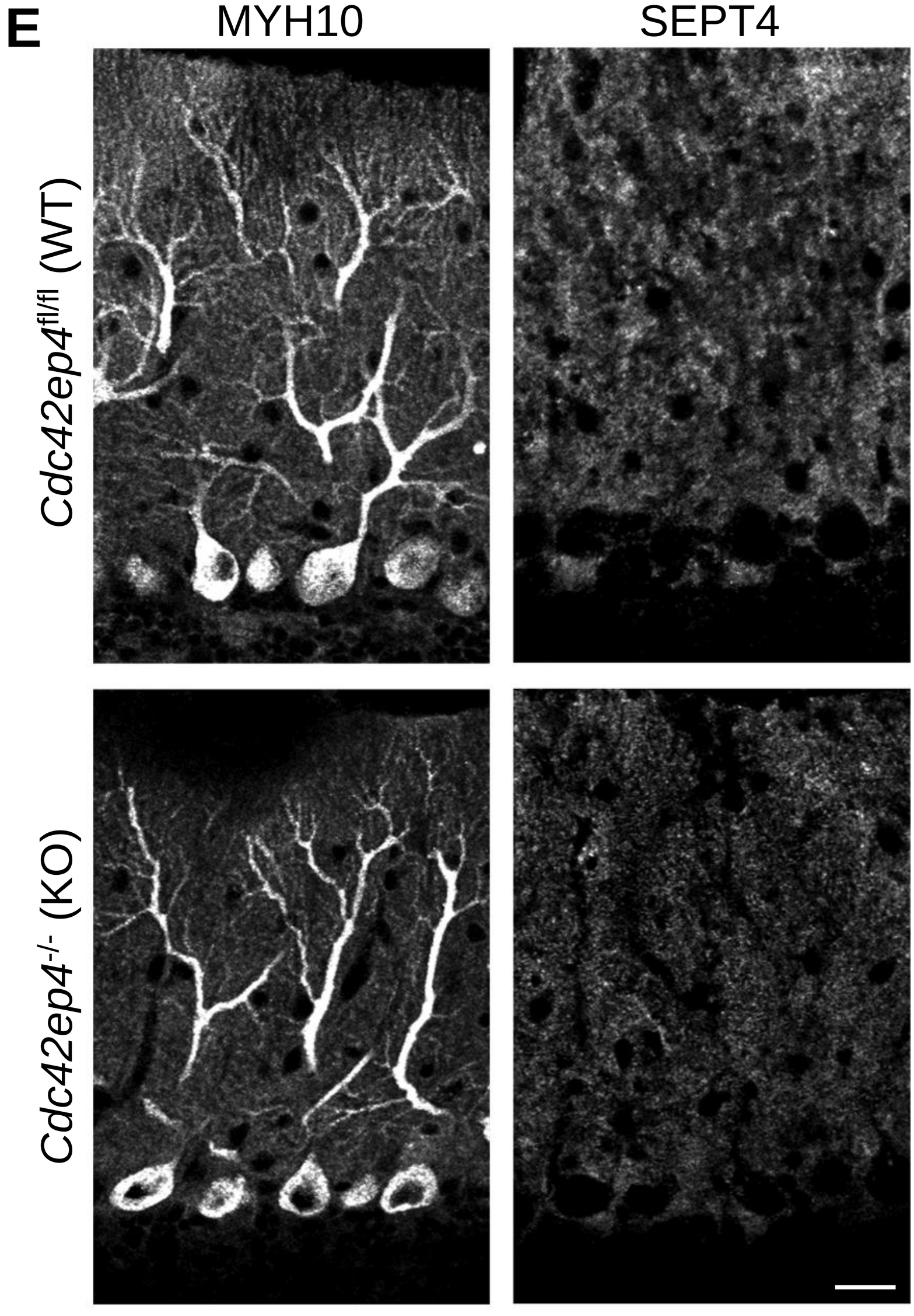
E
MYH10
SEPT4
Cdc42ep4fl/fl (WT)
Cdc42ep4-/- (KO)

A

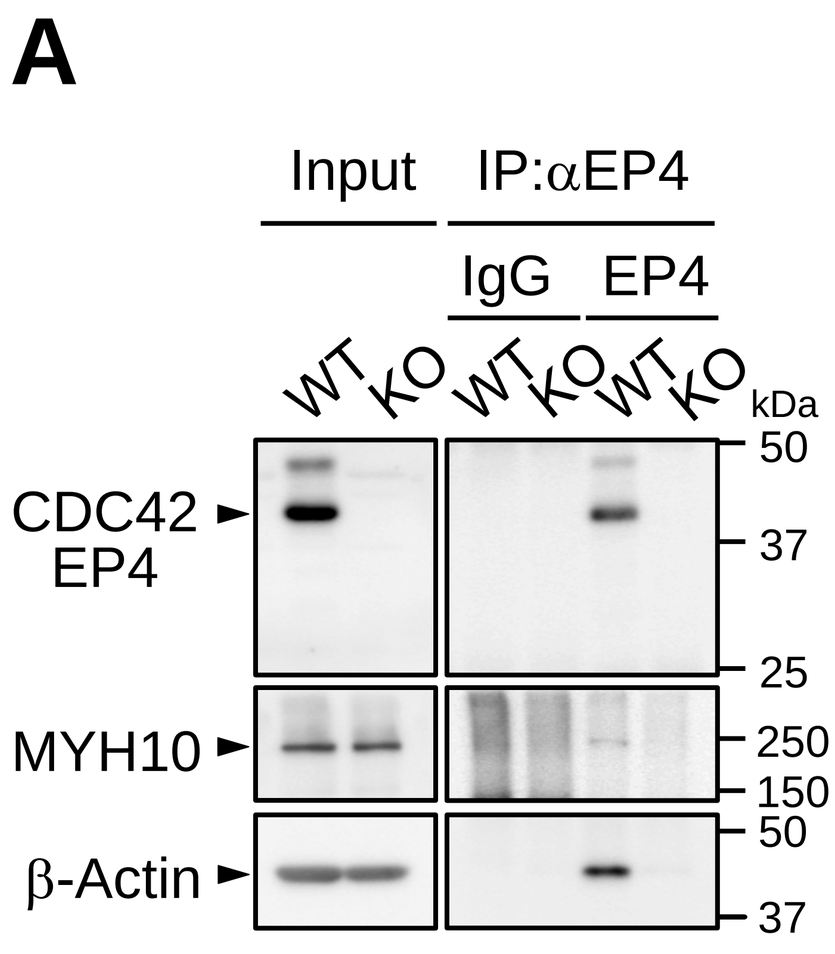
Input
IP:αEP4
IgG
EP4
WT
KO
WT
KO
WT
KO
kDa
CDC42
EP4
MYH10
β-Actin
50
37
25
250
150
50
37

B

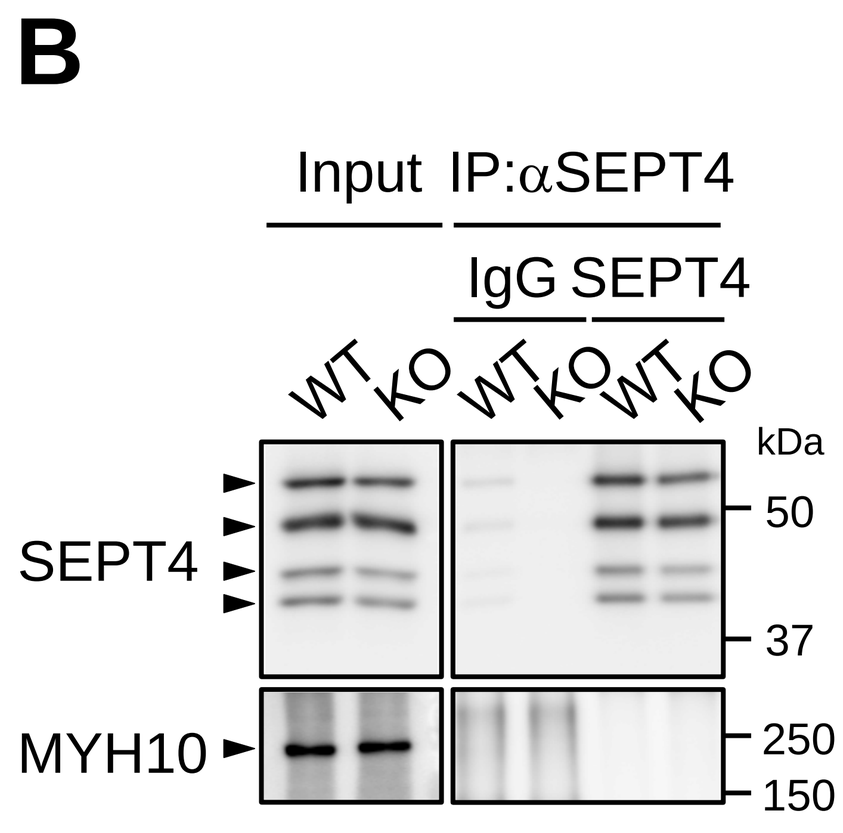
Input
IP:αSEPT4
IgG
SEPT4
WT
KO
WT
KO
WT
KO
kDa
SEPT4
MYH10
50
37
250
150

C

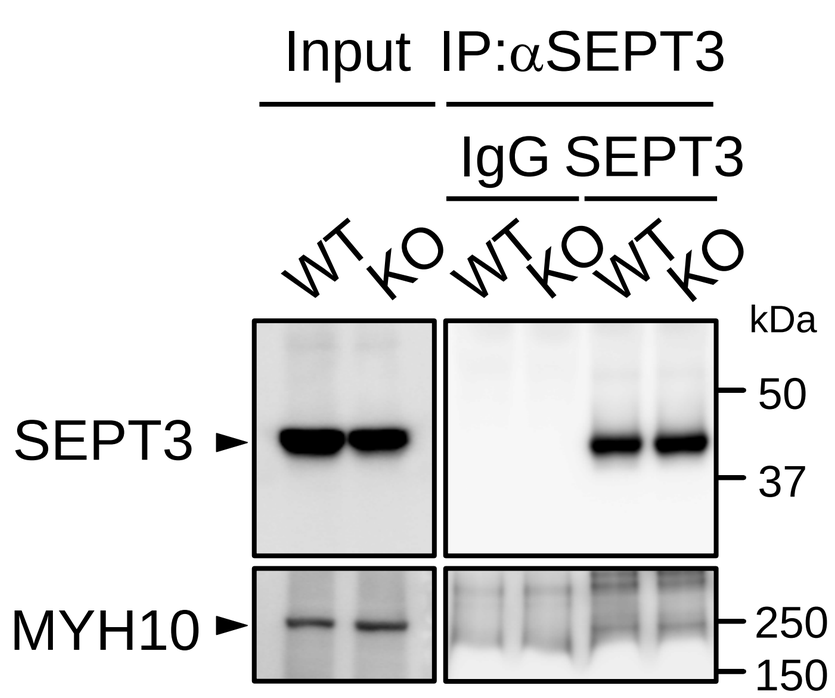
Input
IP:αSEPT3
IgG
SEPT3
WT
KO
WT
KO
WT
KO
kDa
SEPT3
MYH10
50
37
250
150

D

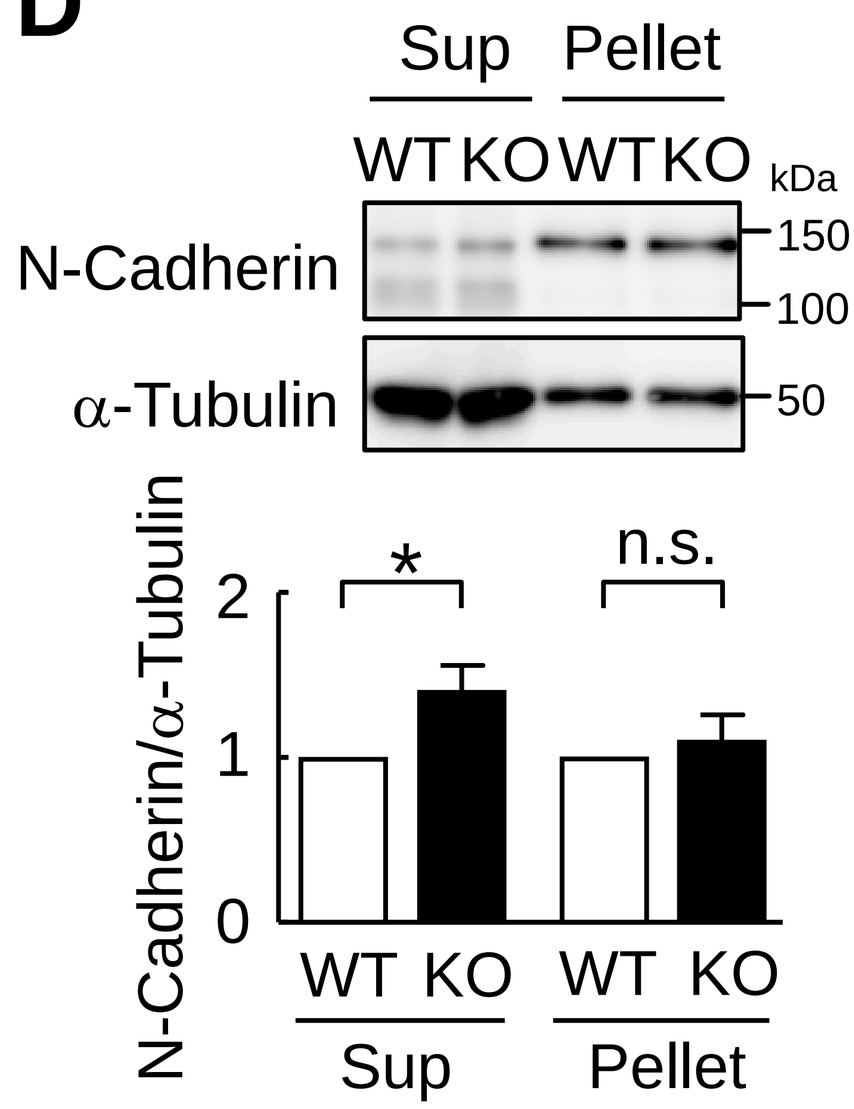
Sup
Pellet
WT
KO
WT
KO
kDa
N-Cadherin
α-Tubulin
150
100
50
N-Cadherin/α-Tubulin
2
1
0
*
n.s.
WT
KO
WT
KO
Sup
Pellet

Supplemental Figure-1